Journal of Solid State Chemistry 183 (2010) 249–254

Contents lists available at ScienceDirect

Journal of Solid State Chemistry

journal homepage: www.elsevier.com/locate/jssc

Neutron diffraction study of phase transitions in perovskite-type strontium molybdate $SrMoO_3$

René B. Macquart [a], Brendan J. Kennedy [a,*], Maxim Avdeev [b]

[a] School of Chemistry, The University of Sydney, Sydney, NSW 2006, Australia
[b] Bragg Institute, Australian Nuclear Science and Technology Organisation, Private Mail Bag 1, Menai, NSW 2234, Australia

ARTICLE INFO

Article history:
Received 11 September 2009
Received in revised form
22 October 2009
Accepted 1 November 2009
Available online 10 November 2009

Keywords:
Perovskite
Phase transition
Neutron diffraction

ABSTRACT

The structure of a polycrystalline sample of $SrMoO_3$ has been investigated using powder neutron diffraction from 5 to 300 K, to reveal two structural phase transitions, the first from the cubic $Pm\bar{3}m$ structure with $a=3.97629(3)$ Å to a tetragonal structure in $I4/mcm$ near 266 K and the second to an orthorhombic *Imma* phase below 125 K. The average Mo–O distance is essentially independent of temperature. The temperature dependence of the octahedral tilting appears typical of a tricritical phase transition.

1. Introduction

The diverse electrical and magnetic properties displayed by ABO_3 perovskites containing a 4*d* transition metal at the octahedral *B*-site is increasingly becoming the focus of interest. Some fifty years after it was first described by Scholder and Brixner [1] $SrMoO_3$, in which the Mo is present as Mo^{4+} with two 4*d*-electrons in threefold degenerate t_{2g} orbitals, is again of interest [2–9], as are the structurally related Ruddlesden–Popper type oxides Sr_2MoO_4 and $Sr_3Mo_2O_7$ [10]. $SrMoO_3$ is commonly described as a cubic perovskite with space group $Pm\bar{3}m$, which exhibits metallic conductivity and Pauli paramagnetism [11,12]. Whilst oxides containing Mo^{4+} generally need to be synthesized in a reducing atmosphere to avoid the formation of the more stable Mo^{6+} (d^0) configuration, the fascinating properties of even simple oxides such as MoO_2 [13] and $Ln_2Mo_2O_7$ [14] more than justify the synthetic effort. Indeed the conductivity of $SrMoO_3$ is amongst the highest of all oxides [15]. Zhao and co-workers showed that doping $SrMoO_3$ with as little as 2.5% Cr to form $SrMo_{0.975}Cr_{0.025}O_3$ is sufficient to drive a transition from the Pauli-paramagnetic state to a ferromagnetic state [7]. The thermoelectric properties of $SrMoO_3$ are equally sensitive to partial oxygen substitution by nitrogen to form $SrMoO_{3-x}N_x$ [4].

Perovskite-type compounds often possess pseudo-symmetry which originates from tilting of the BO_6 octahedra. When the tilting is small it can be difficult to detect using X-ray diffraction, due to the low X-ray scattering power of the oxygen anions. This is especially true for many early studies that relied on laboratory based diffractometers with moderate resolution. There are now numerous examples of oxides, including $SrNbO_3$ [16] and $SrSnO_3$ [17], initially described as cubic perovskites being found to have lower symmetry especially when neutron diffraction methods are employed. Likewise lowering the temperature can induce transitions to lower symmetry as illustrated by $SrCrO_3$ [18] and $SrTiO_3$ [19] both of which become tetragonal upon cooling. Detailed structural studies have now been reported for a number of $SrBO_3$ perovskites where *B* is a 4*d* metal including Zr [20], Nb [16], Ru [21] and Rh [22]. The five oxides $SrBO_3$ (*B*=Zr, Nb, Ru, Rh and Sn) are isostructural at room temperature in the orthorhombic space group *Pnma*. Heating $SrZrO_3$ induces a series of transitions from *Pnma* to *Imma* and $I4/mcm$ and ultimately $Pm\bar{3}m$ [20]. The same sequence of transitions is reported for $SrRuO_3$ [21] and $SrSnO_3$ [17] whereas $SrRhO_3$ [22] decomposes before becoming cubic. To date there do not appear to be any reports of the structure of $SrMoO_3$ at low temperatures, although Brixner reported this remains cubic to 1000 °C [23].

In response to the recent interest in the low temperature electric properties of $SrMoO_3$ and in the expectation that it would exhibit a change in symmetry upon cooling we have investigated the structure of $SrMoO_3$ between 5 and 300 K. We report here the results of high resolution powder neutron diffraction studies that demonstrate the presence of two low temperature phases, one orthorhombic in *Imma* and the second tetragonal in $I4/mcm$.

* Corresponding author.
E-mail address: B.Kennedy@chem.usyd.edu.au (B.J. Kennedy).

0022-4596/$ - see front matter © 2009 Elsevier Inc. All rights reserved.
doi:10.1016/j.jssc.2009.11.005

2. Experimental

$SrMoO_3$ powder was synthesized by mixing stoichiometric quantities of $SrCO_3$ (Aldrich, 99.9+%) and MoO_3 (Aldrich, 99.5+%) with an agate mortar and pestle under acetone, placing the dry mixture in an alumina boat and then heating (850 °C—15 h, 900 °C—15 h, 950 °C—15 h, 950 °C—60 h, 950 °C—15 h, 950 °C—50 h) under flowing H_2(3.5%)/N_2 (one bubble ($\sim$1 cm^3) per second) until phase pure. The sample was reground and X-rayed between heating steps using a PANalytical X'Pert PRO MPD. When synthesized, $SrMoO_3$ has an intense brick red color which turns into a dull red within a few minutes on exposure to air. The sample was stored in an evacuated desiccator when not in use.

Neutron powder diffraction data of a polycrystalline sample of $SrMoO_3$ were measured using the high resolution powder diffractometer Echidna at ANSTO's OPAL facility at Lucas Heights using a wavelength of 1.622 or 2.439 Å [24]. For these measurements the sample was contained in a cylindrical vanadium can which was mounted in a closed cycle helium refrigerator. The synchrotron X-ray diffraction data were collected at ambient temperature in the angular range $5 < 2\theta < 85^\circ$, using X-rays of wavelength 0.82706 Å on the powder diffractometer at BL-10 of the Australian Synchrotron [25]. The sample was housed in a 0.3 mm diameter capillary that was rotated during the measurements. The structures were refined using the program RIETICA [26]. The neutron peak shape was modeled using a pseudo Voigt function and the background was estimated by interpolating between up to 40 selected points.

3. Results and discussion

The synchrotron X-ray diffraction pattern of the deep red sample of $SrMoO_3$ was well fitted in the cubic space group $Pm\bar{3}m$. There was no indication from the refinements against the synchrotron diffraction data for any cation vacancies and the refined lattice parameter of a=3.97632(3)Å is in excellent agreement with previously published values for stoichiometric $SrMoO_3$ [23]. Examination of the synchrotron data showed a number of very weak peaks, the strongest of which had intensity of $\sim$0.1% that of the strongest 1 1 0 reflection of $SrMoO_3$ that could be indexed to some unreacted $SrMoO_4$. There was, however, no evidence for lowering of the symmetry from cubic and as illustrated in Fig. 1 an excellent fit was obtained in $Pm\bar{3}m$. Likewise the neutron diffraction pattern recorded at 300 K was well fitted in the cubic model, and showed the sample to be oxygen stoichiometric within errors of 1–2% in the refined oxygen site occupancies.

Cooling the sample to 250 K resulted in the appearance of a number of additional reflections in the neutron diffraction pattern indicating a lowering of symmetry, Fig. 2. As summarized by Howard and Stokes [27], it is well established that rigid unit rotation of the BO_6 octahedra in perovskites about $\langle 100 \rangle$ corresponds to the freezing of phonons in the cubic Brillouin zone; at the R-point with irreducible representation R_4^+ and/or at the M-point with irreducible representation M_3^+. The mode with wave vector at the M-point describes the rotation of layers of successive octahedra occurring in the same sense (in-phase or +tilts) whilst the R-point mode corresponds to the rotations of layers of successive octahedra in the opposite sense (anti-phase or −tilts). The additional reflections seen in the neutron diffraction data at 250 K could all be accounted for by an R-point mode corresponding to out-of-phase (anti) tilts. The appropriate space group is $I4/mcm$ that has the Glazer [28] notation $a^0a^0c^-$ denoting tilting about the [0 0 1] direction of the aristotype. The neutron patterns recorded at 150 K $\leq T \leq$ 250 K were all well fitted in this model.

Further cooling of the sample below 150 K resulted in a transition to an orthorhombic cell. There was no evidence for any M-point reflections in the neutron pattern obtained below 150 K, and following Howard and Stokes the appropriate space group is $Imma$, corresponding to the tilt system $a^-a^-c^0$, Fig. 3. Structural parameters for the three phases are summarized in Table 1, and the temperature dependence of the lattice parameters obtained from Rietveld analysis is illustrated in Fig. 4. The $Imma$ space group has been observed as an intermediate between $Pnma$ and $I4/mcm$ in a number of $SrBO_3$ perovskites including those with B=Zr, Ru, Rh and Sn. The phase transition from $I4/mcm$ to $Imma$ must be first order since the octahedral rotation axis switches 90° from the pseudocubic [0 0 1] in $I4/mcm$ to [1 1 0] in $Imma$.

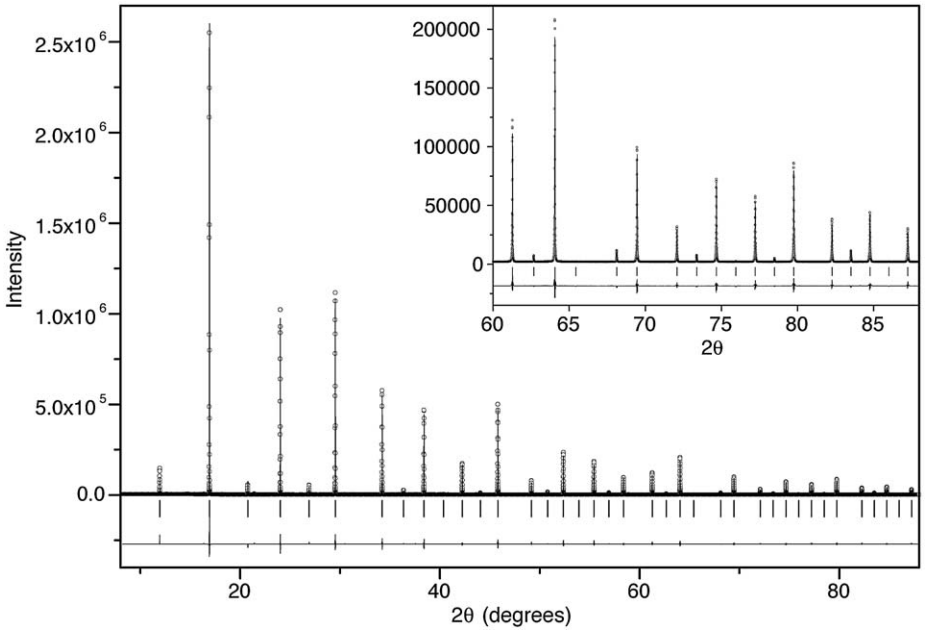

Fig. 1. Powder synchrotron X-ray diffraction pattern for $SrMoO_3$ at 295 K. The observed data are represented by the circles and the solid lines are the results of the Rietveld analysis in cubic $Pm\bar{3}m$. The tick marks correspond to the allowed Bragg reflections. The insert highlights the quality of the data to high angles.

Nevertheless, as evident from Fig. 4 there is no apparent discontinuity in the cell volume at this transition. No magnetic peaks were observed in the neutron diffraction data. Brixner reported that cubic $SrMoO_3$ displays almost linear thermal expansion from room temperature to 1000 °C [23].

The refined Mo–O bond distances are essentially independent of temperature, being about 1.988 Å. This distance is in good agreement with the average Mo–O distance reported recently for $CaMoO_3$, 2.005 Å [29]. The bond valence for the Mo cation, 4.55, is noticeably higher than that expected for a Mo^{4+} cation, but we note a similar anomaly is also reported for $CaMoO_3$ (4.60) [29]. Likewise the BVS for the 12-coordinate Sr^{2+} cation 1.84 is slightly lower than expected. These results suggest that despite the favorable tolerance factor for $SrMoO_3$, $t=(r_{Sr}+r_O)/\sqrt{2}(r_{Mo}+r_O)=0.98$, assuming the

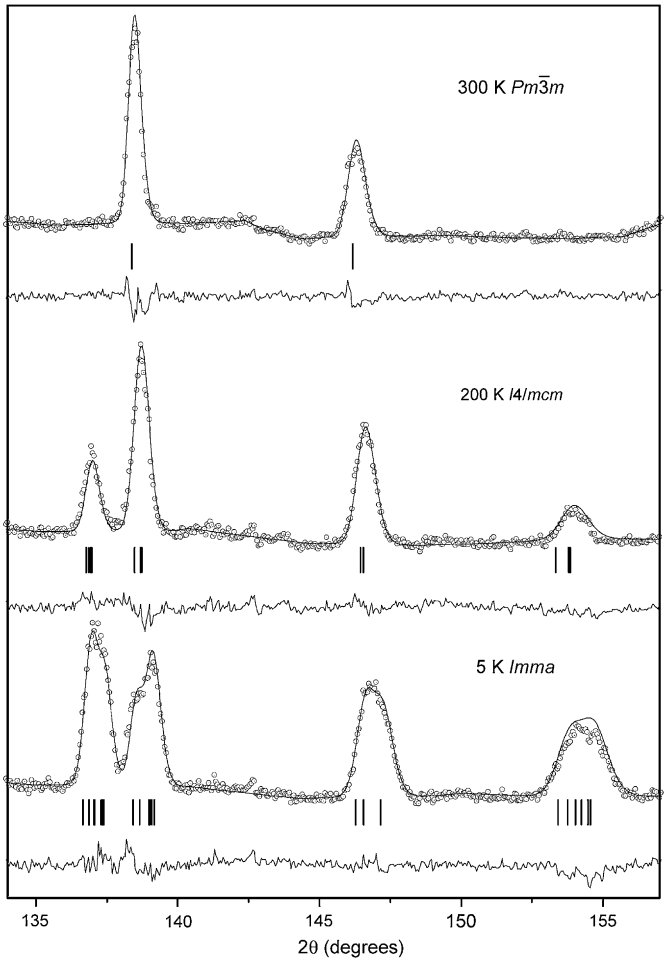

Fig. 2. Portions of the powder neutron diffraction patterns show the presence of diagnostic *R*-point reflections below 250 K.

Table 1
Representative structural parameters for $SrMoO_3$. In all cases the Mo is at the origin (0 0 0) of the appropriate unit cell.

Temperature (K)	5	200	300 neutron	295 synchrotron
Space group	*Imma*	*I4/mcm*	*Pm3̄m*	*Pm3̄m*
a (Å)	5.60897(10)	5.61652(9)	3.97629(3)	3.97609(1)
b (Å)	7.93101(15)	=*a*	=*a*	=*a*
c (Å)	5.62479(10)	7.95239(23)	=*a*	=*a*
Volume (Å^3)	250.217(7)	250.861(9)	62.869(7)	62.860(1)
Sr *x*	0	0	$\frac{1}{2}$	$\frac{1}{2}$
Sr *y*	$\frac{1}{4}$	$\frac{1}{2}$	$\frac{1}{2}$	$\frac{1}{2}$
Sr *z*	0.5010(5)	$\frac{1}{4}$	$\frac{1}{2}$	$\frac{1}{2}$
Sr B_{iso}	0.39(2)	0.59(2)	0.77(3)	0.86(1)
Mo B_{iso} (Å^2)	0.27(3)	0.50(3)	0.55(4)	0.22(1)
O1 *x*	0	0.2364(2)	$\frac{1}{2}$	$\frac{1}{2}$
O1 *y*	$\frac{1}{4}$	$x+\frac{1}{2}$	0	0
O1 *z*	0.0269(5)	0	0	0
O1 B_{iso} (Å^2)	0.34(6)	0.31(2)	0.75(10)	0.99(2)
O2 *x*	$\frac{1}{4}$	0		
O2 *y*	−0.0148(2)	0		
O2 *z*	$\frac{1}{4}$	$\frac{1}{4}$		
O2 B_{iso} (Å^2)	0.71(2)			
Mo–O1 (Å)	1.9828(1) × 2	1.98869(10) × 4	1.98814(1) × 6	1.98805(1) × 6
Mo–O2 (Å)	1.9899(1) × 4	1.98810(6) × 2		
R_p (profile) (%)	7.30	7.78	7.21	6.16
R_{wp} (weighted profile) (%)	10.60	10.98	10.15	9.14
χ^2	2.29	2.85	2.64	60.37

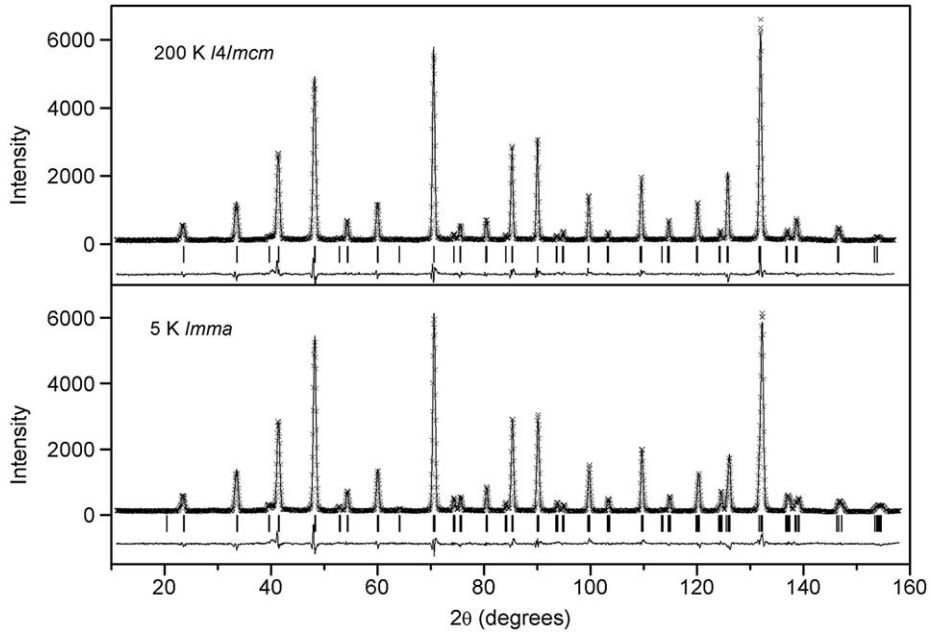

Fig. 3. Powder neutron diffraction pattern for $SrMoO_3$ at 5 K. The data were fitted to a model in the orthorhombic space group *Imma*. The format is the same as in Fig. 1.

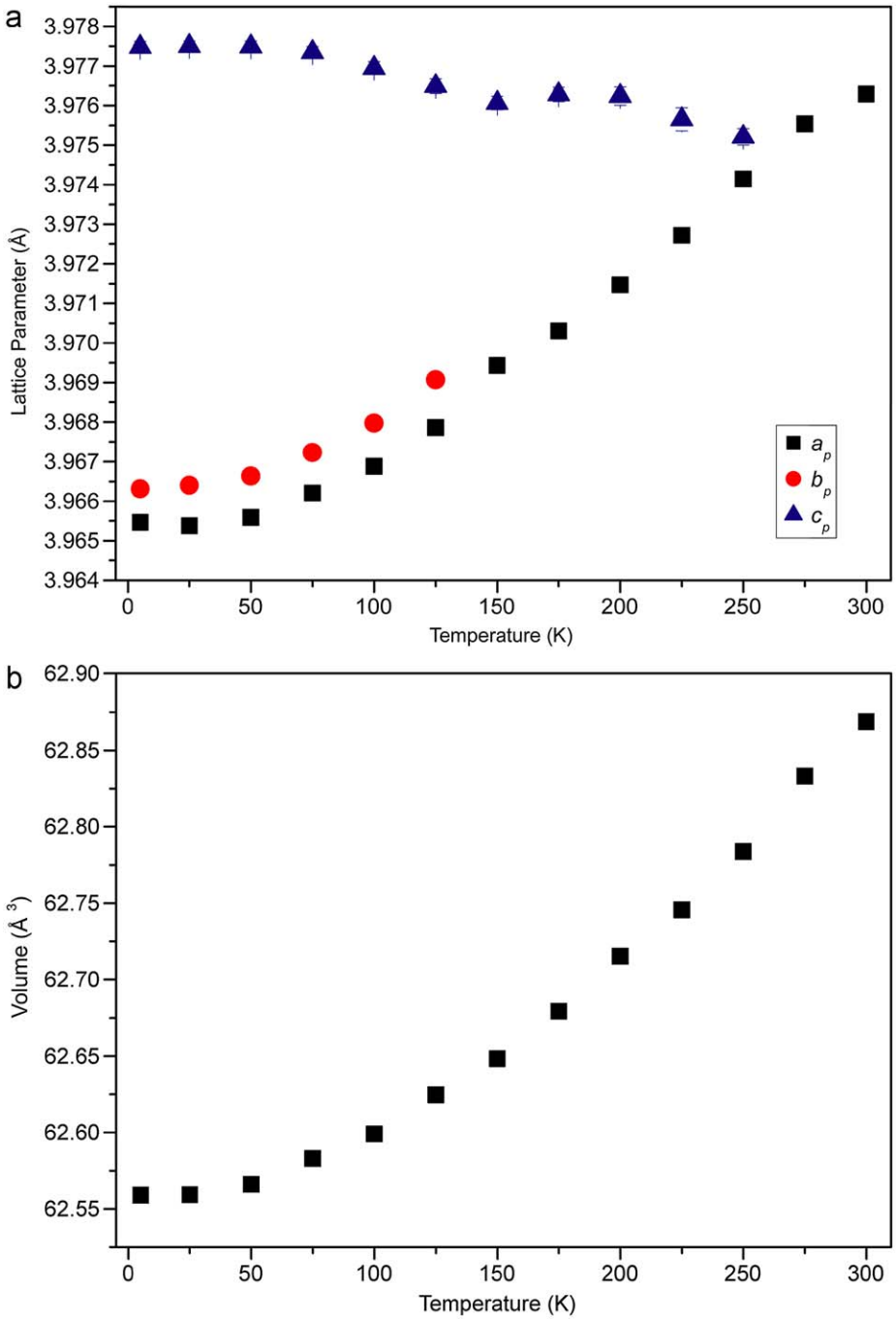

Fig. 4. Thermal evolution of the, appropriately scaled, lattice parameters and cell volume for $SrMoO_3$ obtained from the neutron diffraction measurements.

ionic radii for 6-coordinate Mo^{4+} is 0.650 Å, 12-coordinate Sr^{2+} is 1.44 Å and 6-coordinate O^{2-} is 1.40 Å [30], the Mo is under compressive stress and it is probable that the observed phase transitions act to relieve this.

The tilting around the twofold axis ([1 1 0]), in *Imma* leads to shifts z(O1) of the apical oxygen and y(O2) of the equatorial oxygen atoms. Since the octahedra are not strictly rigid, if they were $z(O1) = -2y(O2)$, we estimate the tilt angle ϕ as the average of $\tan\phi = \sqrt{8}z(O1) + \tan\phi = \sqrt{32}z(O1)$ [31]. The tilting around [0 0 1] in *I*4/*mcm* is estimated as $\tan\phi = 4(0.25 - x(O1))$. The temperature dependence of the tilts is illustrated in Fig. 5 and remarkably there is no obvious discontinuity in this near 150 K corresponding to the first order *Imma*–*I*4/*mcm* transition. There are now a number of examples of perovskites undergoing a first order transition associated with reorientation of the tilting axis in which the magnitude of the tilt is unaffected [31]. For a classical Landau 2–4–6 free energy potential, continuous tricritical transitions will show a monotonic smooth decrease of the tilt angle to zero as the transition temperature (T_c) is approached and the magnitude of the tilt should vary as $(T_c - T)^{0.25}$. Also illustrated in Fig. 5 is the fit to the temperature dependence of the rotation for a $(T_c - T)^{0.25}$ function. The magnitude of the tilt decreases smoothly with the transition temperature being estimated as 266 K and the temperature dependence of this appears typical of a tricritical phase transition.

The transition to the tetragonal structure allows the axial and equatorial Mo–O bond distances in $SrMoO_3$ to be unequal,

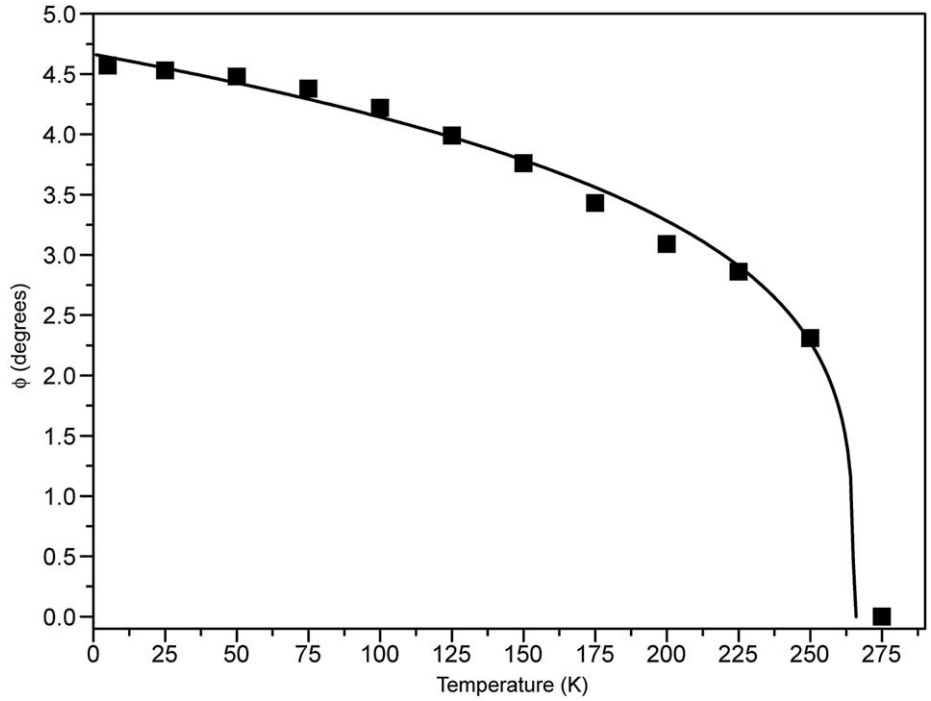

Fig. 5. Temperature dependence of the tilt angle in $SrMoO_3$. The solid line is the best fit to an expression of the form $(T_c–T)^{0.25}$ typical of a tricritical transition where T_c is the temperature of the transition to cubic estimated to be 266 K.

although as is evident from Table 1 these remain essentially equal. Likewise the six Mo–O distances remain approximately equal in the orthorhombic structure. Although the bond distances suggest there is little distortion of the octahedra, as illustrated in Fig. 5, the tilt angles are appreciable at low temperatures.

Comparison of the low temperature phase transitions in the isoelectronic oxides $SrCrO_3$ [18] and $SrMoO_3$ illustrates the remarkable difference between the 4*d* and 3*d* transition metal oxides. Both $SrCrO_3$ and $SrMoO_3$ are cubic at room temperature, but the transition to the tetragonal phase in $SrCrO_3$ is apparently first order and is accompanied by partial orbital ordering [18]. There is no indication, from the refined Mo–O bond distances, for lifting of the orbital degeneracy in the lower symmetry structures of $SrMoO_3$. This is presumably a consequence of the more extended 4*d* orbitals in $SrMoO_3$ [3]. Evidently the cubic–tetragonal–orthorhombic transitions in $SrMoO_3$ do not result in a resistive discontinuity, whereas a correlation between the cubic–tetragonal transition and magnetization is evident in $SrCrO_3$ [18].

4. Conclusion

In summary high resolution powder neutron diffraction studies demonstrate the presence of two low temperature phases in $SrMoO_3$, one orthorhombic in *Imma* and the second tetragonal in *I*4/*mcm*. Although the transition between these must be first order both the cell volume and magnitude of the octahedral tilt angle evolve smoothly through the transition, and the temperature dependence of the tilt angle appears typical of a tricritical phase transition.

Acknowledgments

This work was, in part, performed at the powder diffraction beamline at the Australian Synchrotron. B.J.K. acknowledges the support of the Australian Research Council for this work.

References

[1] R. Scholder, L. Brixner, Z. Naturf. 10 (1955) 178.
[2] S. Hayashi, R. Aoki, T. Nakamura, Mat. Res. Bull. 14 (1979) 409.
[3] Y.S. Lee, J.S. Lee, T.W. Noh, D.Y. Byun, K.S. Yoo, K. Yamaura, E. Takayama-Muromachi, Phys. Rev. B. 67 (2003) 113101.
[4] D. Logvinovich, R. Aguiar, R. Robert, M. Trottmann, S.G. Ebbinghaus, A. Reller, A. Weidenkaff, J. Solid State Chem. 180 (2007) 2649.
[5] T. Maekawa, K. Kurosaki, H. Muta, M. Uno, S. Yamanaka, J. Alloy. Compd. 390 (2005) 314.
[6] H. Mizoguchi, K. Fukumi, N. Kitamura, T. Takeuchi, J. Hayakawa, H. Yamanaka, H. Yanagi, H. Hosono, H. Kawazoe, J. Appl. Phys. 85 (1999) 6502.
[7] B.C. Zhao, Y.P. Sun, S.B. Zhang, W.H. Song, J.M. Dai, J. Appl. Phys. 102 (2007) 113903.
[8] B.C. Zhao, Y.P. Sun, S.B. Zhang, X.B. Zhu, W.H. Song, J. Crystal Growth 290 (2006) 292.
[9] H. Mizoguchi, K. Fukumi, N. Kitamura, T. Takeuchi, J. Hayakawa, H. Yamanaka, H. Yanagi, H. Hosono, H. Kawazoe, J. Appl. Phys. 85 (1999) 6502.
[10] S. Kouno, N. Shirakawa, I. Nagai, N. Umeyama, K. Tokiwa, T. Watanabe, J. Phys. Soc. Jpn. 76 (2007) 3.
[11] I.C. Lekshmi, A. Gayen, M.S. Hegde, Mat. Res. Bull. 40 (2005) 93.
[12] R. Agarwal, Z. Singh, V. Venugopal, J. Alloy. Compd. 282 (1999) 231.
[13] J. Zhou, N.S. Xu, S.Z. Deng, J. Chen, J.C. She, Z.L. Wang, Adv. Mater. 15 (2003) 1835.
[14] B.D. Gaulin, J.N. Reimers, T.E. Mason, J.E. Greedan, Z. Tun, Phys. Rev. Lett. 69 (1992) 3244.
[15] I. Nagai, N. Shirakawa, S. Ikeda, R. Iwasaki, H. Nishimura, M. Kosaka, Appl. Phys. Lett. 87 (2005) 3.
[16] H. Hannerz, G. Svensson, S.Y. Istomin, O.G. D'yachenko, J. Solid State Chem. 147 (1999) 421.
[17] M. Glerup, K.S. Knight, F.W. Poulsen, Mat. Res. Bull. 40 (2005) 507.
[18] L. Ortega-San-Martin, A.J. Williams, J. Rodgers, J.P. Attfield, G. Heymann, H. Huppertz, Phys. Rev. Lett. 99 (2007) 255701.
[19] G. Shirane, Y. Yamada, Phys. Rev. 177 (1969) 858.
[20] C.J. Howard, K.S. Knight, B.J. Kennedy, E.H. Kisi, J. Phys. Conden. Matter 12 (2000) L677.
[21] B.J. Kennedy, B.A. Hunter, J.R. Hester, Phys. Rev. B. 65 (2002) 2241031.
[22] B.J. Kennedy, K. Yamaura, E. Takayama-Muromachi, J. Phys. Chem. Solids 65 (2004) 1065.
[23] L.H. Brixner, J. Inorg. Nucl. Chem. 14 (1960) 225.
[24] K.D. Liss, B. Hunter, M. Hagen, T. Noakes, S. Kennedy, Physica B 385–386 (2006) 1010.

[25] K.S. Wallwork, B.J. Kennedy, D. Wang, AIP Conference Proceedings, vol. 879, 2007, p. 879.
[26] B.A. Hunter, C.J. Howard, in: A Computer Program for Rietveld Analysis of X-ray and Neutron Powder Diffraction Patterns, Lucas Heights Research Laboratories, Sydney, 1998, p. 1.
[27] C.J. Howard, H.T. Stokes, Acta Cryst. B 54 (1998) 782.
[28] A.M. Glazer, Acta Cryst. B 28 (1972) 3384.
[29] C. de la Calle, J.A. Alonso, M. Garcia-Hernandez, V. Pomjakushin, J. Solid State Chem. 179 (2006) 1636.
[30] R.D. Shannon, Acta Cryst. A 32 (1976) 751.
[31] M.A. Carpenter, C.J. Howard, B.J. Kennedy, K.S. Knight, Phys. Rev. B 72 (2005) 15.